Automation and low cost proteomics for characterization of the protein corona: Experimental methods for big data

Karsten M. Poulsen,[†] Thomas Pho,[¶] Julie A. Champion,^{¶,*} Christine K. Payne^{†,*}

[†]Department of Mechanical Engineering and Materials Science, Duke University, Durham, NC 27708, USA. [¶]School of Chemical and Biomolecular Engineering, Georgia Institute of Technology, Atlanta, GA 30332, USA and the Parker H. Petit Institute for Bioengineering and Biosciences, Georgia Institute of Technology, Atlanta, GA 30332, USA.

*e-mail: julie.champion@chbe.gatech.edu, christine.payne@duke.edu

Abstract

Nanoparticles used in biological settings are exposed to proteins that adsorb on the surface forming a "protein corona." These adsorbed proteins dictate the subsequent cellular response. A major challenge has been predicting what proteins will adsorb on a given nanoparticle surface. Instead, each new nanoparticle and nanoparticle modification must be tested experimentally to determine what proteins adsorb on the surface. We propose that any future predictive ability will depend on large data sets of proteinnanoparticle interactions. As a first step towards this goal, we have developed an automated workflow using a liquid handling robot to form and isolate protein coronas. As this workflow depends on magnetic separation steps, we test the ability to embed magnetic nanoparticles within a protein nanoparticle. These experiments demonstrate that magnetic separation could be used for any type of nanoparticle in which a magnetic core can be embedded. Higher-throughput corona characterization will also require lower cost approaches to proteomics. We report a comparison of fast, low-cost, and standard, slower, higher-cost, liquid chromatography coupled with mass spectrometry to identify the protein corona. These methods will provide a step forward in the acquisition of the large data sets necessary to predict nanoparticle-protein interactions.

Introduction

Nanoparticles (NPs) used in any "real world" application encounter a range of molecules that will adsorb on the surface of the NP [1-10]. These adsorbed molecules, referred to as a "corona," determine how the NP functions in downstream applications. The majority of studies in this area have focused on the protein corona that forms when NPs, often developed for nanomedicine applications, interact with blood serum proteins. This protein corona is responsible for subsequent NP-cell interactions including NP clearance from circulation and accumulation in the liver and spleen [11-16]. More recently, the study of biomolecular coronas has been expanded to include lipids and metabolites [17-19]. Beyond these nanomedicine applications, NPs used as anti-microbials, fertilizers, pesticides, and agricultural sensors directly interact with the molecules found in water and soil environments [20-26].

Currently lacking in this research area is the ability to predict what molecules will adsorb on the surface of a NP. Instead, each new NP and surface modification requires an experiment to identify the adsorbed proteins. These experiments consist of incubating NPs and proteins to form a protein corona, removing unbound and weakly bound proteins from the solution, and then carrying out proteomics to identify the adsorbed proteins. This workflow has been described in detail recently [10]. Computational approaches have made progress in terms of predicting the structure of individual proteins as they interact with NP surfaces [27-40], but the ability to predict which protein within a protein mixture will adsorb on the surface of specific NP is not yet possible.

The ability to predict what proteins will adsorb on the surface of NPs would have major implications for the nanomedicine community by saving the time and money associated with experiments. In addition, any methods developed for this community could be extended to the environmental and other NP communities, facilitating work in these areas. To be able to predict what proteins will adsorb on the surface of NPs, we need much larger data sets than are typically used. Most research, including our own [41-44], has tried to predict protein adsorption by working with groups of 2-5 NPs with, for example, varied surface charge, but the small sample size has made it difficult to predict protein

adsorption. W.C.W Chan and co-workers synthesized and characterized a library of 105 gold NPs using 3 different gold cores (15 nm, 30 nm, 60 nm) and 67 different ligands (small molecules, polymers, peptides, surfactants) [45]. This size of data set is ideal for corona prediction, but this level of effort and the cost of proteomics for this many samples is outside the scope of many labs.

We identified two steps in the protein corona experimental workflow where time and/or costs could be reduced to enable higher-throughput, lower-cost, experiments that would allow for the acquisition of larger data sets. The first is the use of an automated liquid handling robot to form and isolate protein coronas. Using a relatively low-cost liquid handler (~\$5000 USD), this allows for a significant decrease in human experimental time. The second area is proteomics cost, working with the proteomics core facility to identify lower cost options that provide the necessary sensitivity for corona experiments. Experimental methods and outcomes for each are described below with a comparison between high-throughput and lower cost approaches with standard lab protocols.

We expect that these approaches can be used to generate large data sets that will be essential to recent machine learning efforts in the protein corona community [46,47]. Robotics have been used previously for the automated synthesis of colloidal NPs [48]. Used in combination with the approaches described below, one could imagine a completely automated workflow with embedded machine learning for optimization [49].

Materials and Methods

Nanoparticles (NPs)

Three types of NPs were used in the course of experiments. Magnetic NPs (magNPs, 200 nm, carboxylate-modified, #SC0202, Ocean NanoTech, San Diego, CA) were used for automation experiments. Small magnetic NPs, referred to as iron oxide NPs (IONPs, 10 nm, methyl-modified, #IO-A10-5, Cytodiagnostics, Burlington, ON, Canada), were used as core NPs in the protein NPs, described below. Polystyrene NPs (200 nm, carboxylate-modified, #F8806, Life Technologies, Carlsbad, CA) were used for

proteomics experiments. The polystyrene NPs were chosen for proteomics as well-characterized, well-behaved NPs, for testing new proteomics protocols [41,43,50-53].

Protein NP synthesis

Ovalbumin (OVA) NPs were prepared using a modified desolvation method [54,55]; 0.4 mL ethanol was added at a constant rate of 0.5 mL/min to 0.1 mL of 22 mg/mL OVA (#A5503, Thermo Fisher Scientific, Waltham, MA) in phosphate buffered saline (PBS, pH 7.4) under constant stirring at 600 rpm. The protein NPs were collected by centrifugation and resuspended by sonication in 0.5 mL PBS. 2.5 µL of a 50-fold dilution of glutaraldehyde (#G7651, Thermo Fisher) was added to stabilize the protein NPs and stirred for one hour at room temperature. The protein NPs were centrifuged at 14,000 xg and resuspended in 0.750 mL PBS.

Iron oxide nanoparticle (IONP)-doped protein NP synthesis

OVA protein NPs loaded with IONPs were prepared following a similar desolvation method. Methyl-functionalized IONP were sonicated and 10 μ L of 5 mg/mL IONP were added to 0.1 mL of 22 mg/mL OVA and stirred briefly. The ethanol desolvation and glutaraldehyde crosslinking were performed exactly as described above for the undoped protein NPs. IONP-protein NPs were collected by centrifugation at 18,000 xg, resuspended in 0.5 mL PBS and separated using a neodymium magnet (#NB041, Applied Magnets, Plano, TX).

NP characterization

Transmission electron microscopy (TEM) for magNP and polystyrene NP characterization used a Tecnai G² TWIN (FEI, Hillsboro, OR) at the Shared Materials Instrumentation Facility at Duke University. MagNP images were obtained at 160 kV with 25 kX magnification and polystyrene NPs at 120 kV with 20 kX magnification. TEM for protein NPs was carried out on a CX-100 (JEOL, Akishima, Japan) TEM, part of the core facilities at the Georgia Institute of Technology. Protein NP images were obtained at 100 kV with 80 kX magnification. All samples were prepared by drop casting on 400 mesh copper grids (#CF400-Cu, Electron Microscopy Sciences, Hatfield Township, PA) and dried at

room temperature. Protein NPs were also stained with 5 μ L of 1% sodium phosphotungstate (#496626, Thermo Fisher) solution and washed twice with Milli-Q water. Particle diameters were measured with ImageJ [56]. Average and standard deviation are reported for all measurements.

Hydrodynamic diameter, polydispersity index, and zeta potential of the magNPs (400 μg/mL in water), polystyrene NPs (8 pM in water), and protein NPs (2.93 mg/mL in PBS for size, 0.293 mg/mL in 10% PBS for zeta potential) were measured using dynamic light scattering (DLS; Malvern Zetasizer, Nano-Z, Malvern Instruments, Worchestershire, England). Measurements were carried out in triplicate with three distinct samples. Each measurement consisted of 12 - 30 runs. Average and standard deviation are reported for all measurements. Electrophoretic mobility was converted to a zeta potential using the Smoluchowski approximation.

Liquid handling robot

A liquid handling robot (OT-2, Opentrons, Brooklyn, NY) with additional electromagnet and temperature modules was used to automate protein corona formation and isolation. Experimental protocols were written in python using Opentrons API v2.1. Pipette tips (20 µI, single and 300 µI, multi) and tipracks used were purchased from Opentrons to verify compatibility and calibration. To run each protocol, the robot was calibrated in the x, y and z directions, followed by calibrating the location of each piece of labware. The locations of each reagent and sample were designated in the script and appropriately positioned after the robot was calibrated. Labware not provided from Opentrons includes a tube rack with base and a water trough. The tube rack and base were 3D printed (3 mm polylactic acid, Ultimaker 2, Utlimaker, Geldermalsen, Netherlands) and the g-code was prepared using Cura (v4.4.1, Ultimaker). The designs for the tube rack were published on thingiverse by *thehair*.

Protein analysis

The protein corona was formed by incubating NPs, both magNPs and polystyrene NPs, with 10% fetal bovine serum (FBS, #10437028, Thermo Fisher). For automation of

experiments, the protein concentration in each wash step was determined by absorbance at 280 nm using a plate reader (SpectraMax iD3, Molecular Devices). UV transparent plates were used for all experiments in order to measure absorption at 280 nm. In practice, less expensive, non-transparent, plates could be used once the number of wash steps had been determined. Absorbance at 280 nm was converted to protein concentration using an extinction coefficient of 43,824 M⁻¹ cm⁻¹, the value for bovine serum albumin. While FBS is a mixture of many different proteins, albumin is the most abundant (55%). As a technical note, bicinchoninic (BCA) assays are not directly compatible with the magNPs due to interaction of the copper reagent with the iron oxide of the NPs [57,58]. Average and standard deviation are shown. P values were calculated using a two-tailed Student's *t*-test.

Gel electrophoresis was used to image individual proteins present in the hard corona of the magNPs. MagNPs with hard coronas (16 μL) were heated in loading buffer (Laemmli loading buffer, #BP-110R, Boston BioProducts, Ashland, MA) for 5 min at 95 °C and then loaded onto a gel (tris-glycine sodium dodecyl sulfate (SDS) gel, #4561093, Bio-Rad, Hercules, CA) for SDS-polyacrylamide gel electrophoresis (PAGE; 230 V, 35 min). A 10 to 250 kDa molecular weight marker (Precision Plus Protein Dual Color Standards, #1610374, Bio-Rad) was included. Gels were rinsed by microwaving in deionized water (1 min heat, 1 min rocking at room temperature, replace water, x3) and then stained (SimplyBlue Safe Stain, #LC6060, Thermo Fisher) by microwaving until near boiling (1 min) and then rocked for 5 min. The gel was rinsed in deionized water (10 min, rocking) and NaCl solution (20% w/V, >5 minutes, rocking) and then imaged (PhotoDoc-It, Analytik Jena, Jena, Germany). ImageJ was used for densitometric analysis (Gel Analyzer) and profile plots (Plot Profile) [56].

Proteomic analysis was carried out in the Proteomics and Metabolomics Core Facility, part of the Duke Center for Genomics and Computational Biology. A protein corona was formed on polystyrene NPs using previously published protocols [41,43,50-53]. A BCA assay (#23250, Thermo Fisher) was used to determine protein concentration. The protein-NP sample was processed by the Core Facility including in-solution trypsin digest

and addition of an internal standard of yeast alcohol dehydrogenase (#186002328, Waters Corporation, Milford, MA) for quantification. This single sample was then analyzed, in triplicate, using two different liquid chromatography (LC) instruments, referred to as MicroFlow and NanoFlow for a total of 6 experiments. MicroFlow LC used a 1 mm x 100 mm ultra-performance liquid chromatography (UPLC, M-Class, Waters Corporation; 80 μL/min) column with a 17 minute total elution time. NanoFlow LC used a 75 μm x 250 mm UPLC column (nanoAcquity, Waters Corporation; 400 nL/min) with a 60 minute total elution time. Both methods use an acetonitrile gradient (5-40%) with 0.1% formic acid. Peptide fragments were analyzed using in-line tandem mass spectrometry (Orbitrap Fusion Lumos, Thermo Fisher). Data was analyzed using Mascot (v. 2.5.1, Matrix Science, Boston, MA) and Scaffold (v. 4.10.0, Proteome Software, Portland, OR). A detailed description of the Core protocol is provided in Supporting Information.

Results and Discussion

NP Characterization

DLS (3 distinct samples) and TEM were used to characterize the NPs used for experiments (Table 1 and Figure 1).

Table 1. Characterization of NPs.

NPs	d _h (nm)	PDI	ZP (mV)	TEM (nm)
magNPs #SC0202	260 ± 2	0.13 ± 0.02	-32 ± 4	129 ± 43 n = 85
IONPs #IO-A10-5	9.48 ± 1	0.20 ± 0.01	-38 ± 3	10.5 ± 1.3 n = 71
polystyrene NPs #F8806	307 ± 2	0.10 ± 0.02	-36 ± 0.5	241 ± 77 n=50

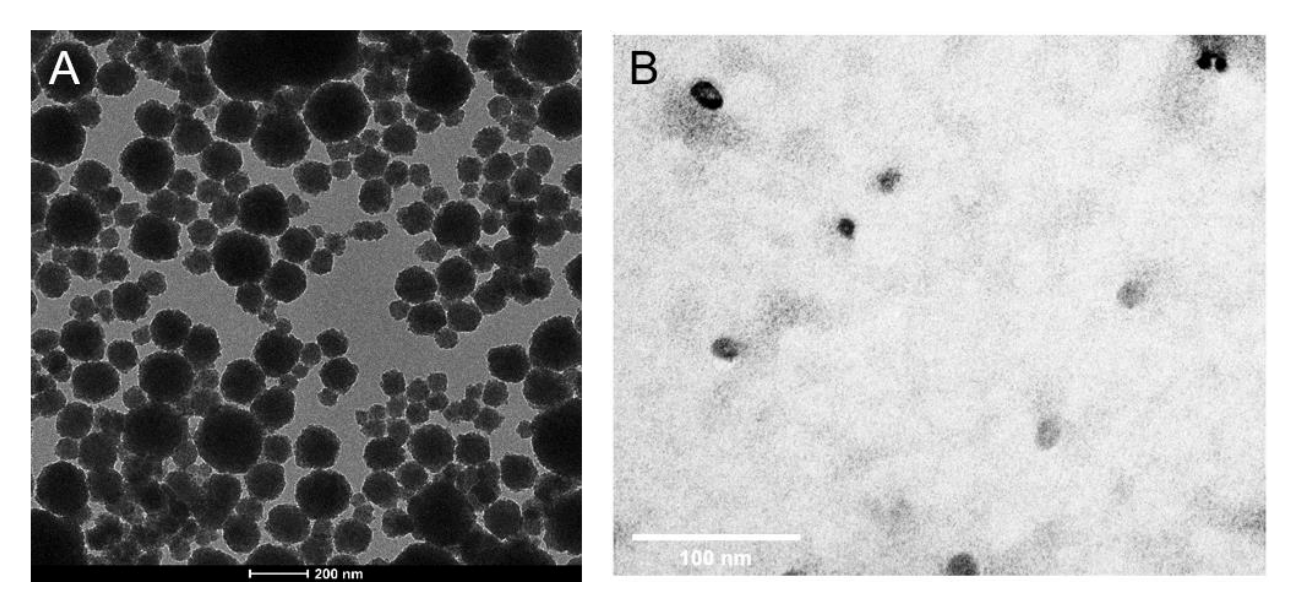


Figure 1. TEM images of magnetic NPs. A. MagNPs used in automation experiments. Scale bar is 200 nm. B. IONPs used as magnetic cores in protein NPs. Scale bar is 100 nm.

Carboxylate-modified polystyrene NPs, which are well-behaved NPs that have been characterized extensively in the Payne Lab [41,43,50-53], were used for proteomics experiments. A TEM image of the polystyrene NPs has been published previously along with the DLS and TEM values (Table 1) [53].

Protein Corona Formation and Characterization

The use of a liquid handling robot is expected to increase throughput and reproducibility in protein corona formation and characterization. Translating experiments done by a person to the robot includes changing the separation steps used to remove unbound and weakly bound proteins and isolate the hard corona. Our lab, and many others, uses centrifugation to pellet the NPs and remove the supernatant. The NPs are then resuspended in water or buffer and this step is repeated until no protein is detected in the supernatant, typically measured by BCA assay. The protein that remains bound to the NPs is defined as the hard corona. Moving samples to a centrifuge, even in a 96-well format, is a bottleneck in the workflow. Instead, we use a magnetic base within the robot frame to separate NPs from proteins using a similar washing process, but with a magnetic pull down step in place of centrifugation. This does require using magNPs either as standalone NPs or as a magnetic core embedded within an NP of interest, as described below.

The protein corona was formed by incubating magNPs (3.2 g/L) with 10% FBS in PBS for a total volume of 250 μL. FBS was chosen as the recommended protein nutrient source for many cell lines, making these results immediately relevant to in vitro experiments. All protocols described in this manuscript could also be used for human, or other, serums. Experiments were carried out in 96-well plates working with 8 samples simultaneously. Corona formation, resulting in protein-magNP complexes, was carried out at room temperature for 30 minutes with automated mixing by pipetting up and down every 3 minutes during the 30 minute incubation. Removal of unbound and weakly bound proteins, typically referred to as "washing" in the protein corona community, was carried out using a magnetic base module to separate the protein-magNPs from the proteins in solution. The washing process was initiated by engaging the magnetic base, removing 80% of the volume (200 μL) in each well and replacing it with an equal volume of PBS. For each resuspension the solution was mixed by pipetting up and down (150 µL x3) by the robot. For the first wash, we waited 10 min prior to removing solution to allow time for pull down of the magNPs. Subsequent wash steps used 5 min incubations. The solution that was removed at each wash step was saved for analysis to measure protein concentration (Figure 2).

The goal of the wash process is to identify the wash step at which all unbound and weakly bound protein has been removed, with only NP-bound protein remaining. The protein concentration in each wash step was determined by absorbance at 280 nm using a plate reader. Absorbance at 280 nm was converted to protein concentration (ε = 43,824 M⁻¹ cm⁻¹) using Beer's Law. After 4 washes, there is no statistical difference between the subsequent wash solutions (Figure 2). The concentration of the magNPs is also confirmed at this point, as it is possible to lose NPs during wash steps. We measure magNP concentration by absorption at 330 nm and comparison to a calibration curve with known concentrations. We observed a 4.2 ± 2.4% (n=8) loss after 10 wash steps. After 5 wash steps, we used gel electrophoresis to characterize the proteins present in the hard corona of the magNPs (Figure 3 and S1). Densitometric analysis of the two prominent bands at ~70 kDa and ~125 kDa shows that these two bands have average intensities of

 3.0 ± 0.5 and 1.3 ± 0.3 , respectively. While the standard deviation is relatively low, 17% and 23%, respectively, future experiments will determine the source of this variability.

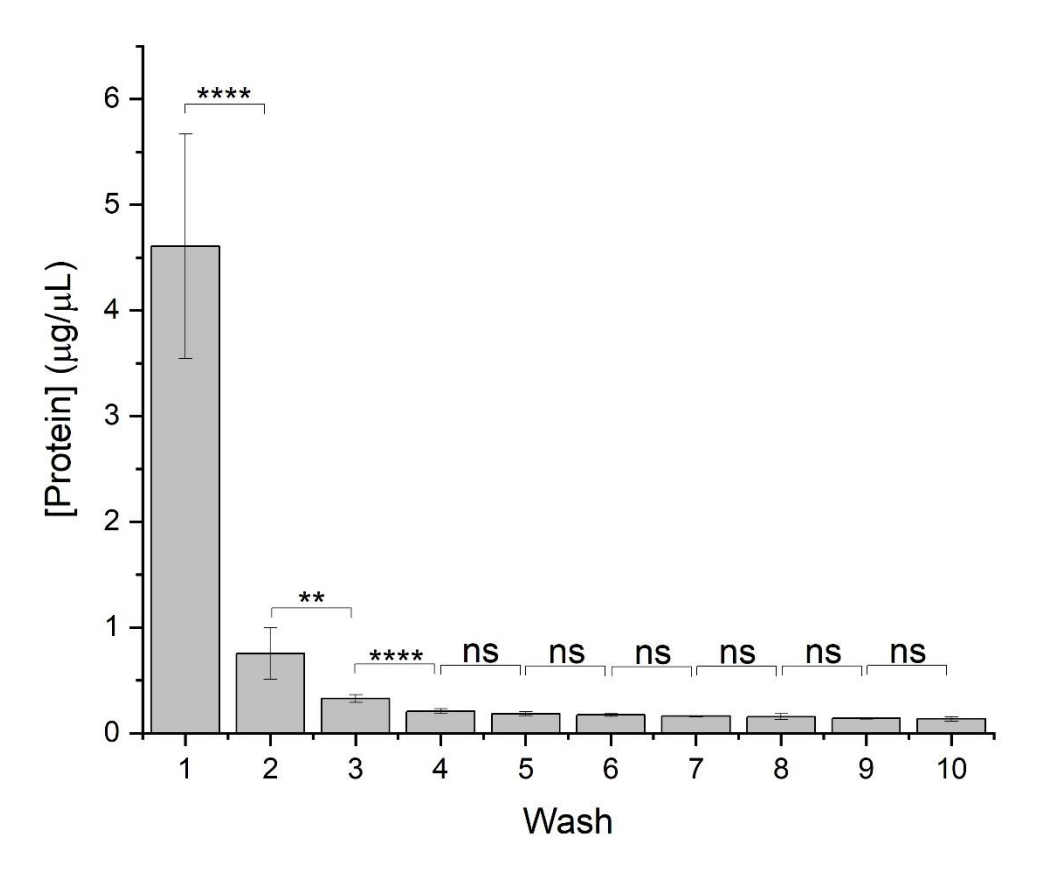


Figure 2. Protein concentration ($\mu g/\mu L$) measured at each wash step. n=8; ****p<0.0001, **p<0.01, ns=non-significant.

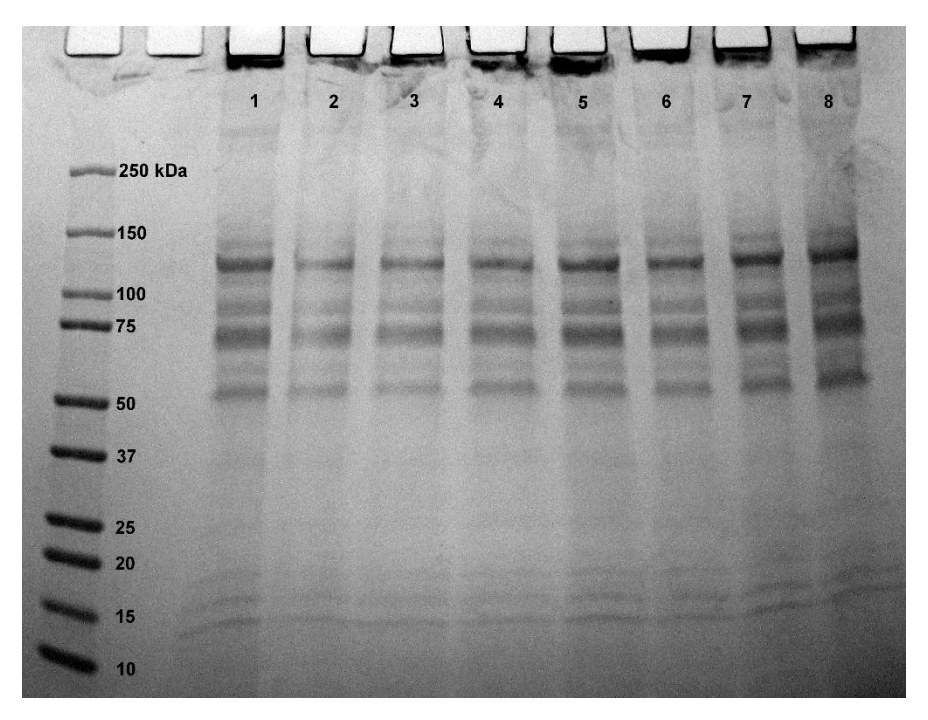


Figure 3. Gel electrophoresis of the hard corona adsorbed on magNPs. A profile plot of each lane is shown in Fig. S1.

An immediate advantage of the use of the liquid handling robot is the time saved by the human researcher. Preparing the robot for a run includes placement of labware and calibration of tips, which takes ~3 minutes of human time. To complete the 5 wash steps to isolate a hard corona requires 66 minutes of robot time, which includes protein-NP incubation, pipetting to mix wells, pull downs, and transferring samples between wells. In comparison, we estimate that preparing 8 samples by hand, working with a multi-channel pipettor and centrifugation, would require 30 minutes of active human time and 75 minutes of waiting (30 min incubation, 15 minute centrifugation x3). Using magnetic pull down instead of centrifugation would decrease waiting times, but does not change the time necessary for a human to mix and transfer samples.

Protein NPs with Magnetic Cores

Although this automated workflow does require magnetic NPs, magnetic NPs can be modified to vary surface properties or can be embedded within another material. Surface properties, rather than the composition of the NP core, control protein corona formation

[44,45,59]. For example, our previous work compared the corona-mediated cellular response to iron oxide and polystyrene NPs functionalized with the same carboxymethyl dextran ligand and found that the ligand, rather than the NP core, was the key feature [44]. To demonstrate that magnetic NPs could be embedded within another material, we fabricated OVA protein NPs by desolvation with and without magnetic iron oxide NPs (IONPs) embedded inside. OVA NPs were chosen since these are model vaccine nanoparticles. This platform is highly tunable and has been used for a variety of proteins, such as influenza antigens [55,60,61].

IONPs, ~20x smaller than the protein NPs, were selected so they would be trapped within the protein NPs instead of simply adsorbing the OVA proteins on their surface. For sufficient magnetic strength, multiple IONPs need to be embedded in each NP. IONPs were incorporated within OVA NPs, as indicated by TEM (Figure 4). The IONPs appeared to be clustered within the NP.

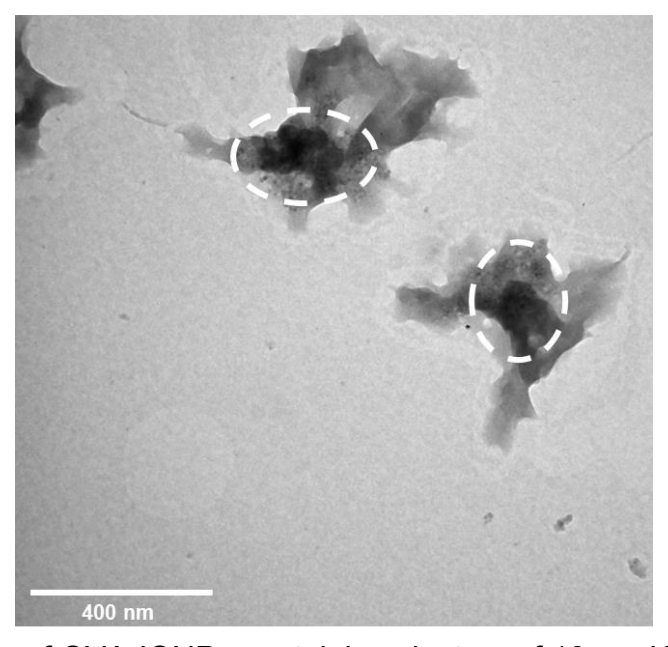


Figure 4. TEM image of OVA-IONPs containing clusters of 10 nm IONPs (white ovals). Scale bar 400 nm.

Statistical analysis of DLS and zeta potential measurements indicated that there was no difference in OVA NP size and surface charge with the embedded IONPs (Table 2, Figure

S2 and S3). The hydrodynamic diameters for OVA and IONP-OVA NPs were 274 ± 16 and 251 ± 27 nm, respectively (p = 0.5363). Zeta potentials were -27 ± 2 mV and -26 ± 1 mV, respectively (p = 0.8955). In comparison, the IONPs had a hydrodynamic diameter of 9.48 ± 0.80 nm and a zeta potential of -38.3 ± 3.0 mV (Table 1). The IONP-OVA NPs were easily separated from solution with a small magnet, indicating they can be used in the same high-throughput protein corona workflow. All characterization of IONP-OVA NPs was performed after magnetic separation and resuspension.

Table 2. Characterization of protein NPs.

NPs	d _h (nm)	PDI	ZP (mV)
OVA NP	274 ± 16	0.31 ± 0.05	-27 ± 2
IONP-OVA NP	251 ± 27	0.22 ± 0.06	-26 ± 1

Low Cost Proteomic Analysis of the Protein Corona

Duke's Proteomics Core Facility, and likely that of other core facilities, uses the time necessary for an experiment to set the cost for staff support and reagents. This means that faster experiments lead to lower user fees. In the case of the liquid chromatography (LC) and mass spectrometry (MS) used for protein corona analysis (LC-MS/MS), the use of high flow LC systems (MicroFlow) can decrease the time, and price, of the experiments by a factor of 2 compared to NanoFlow LC, which is the standard method in our Core. The subsequent mass spectrometry is identical for both separation methods. Our analysis of the corona formed on polystyrene NPs using both LC systems, with identical samples, showed that of the 25 most abundant proteins identified in the corona, 23 were identified using both LC methods.

The most abundant protein identified by both LC methods was complement C3. Despite being the most abundant protein in serum, serum albumin was only the 14th most abundant protein adsorbed on the surface of the polystyrene NPs. This result, with complement C3 dominating the corona, is similar to previous proteomics analysis of nearly identical carboxylate-modified polystyrene NPs (200 nm) carried out in 2015 [50],

which differed only in the fluorophore. Previous results also showed that the corona increases the hydrodynamic diameter of carboxylate-modified polystyrene NPs and decreases the zeta potential, reflecting the charge of the adsorbed protein [41]. The relative enrichment of complement C3 and depletion of albumin in the corona has also been observed by our lab with titanium dioxide NPs [50], and by others working with gold nanoparticles [45], iron oxide nanoparticles [62], and iron oxide nanoworms [63]. While this observation points towards the importance of complement C3 as an immune protein recognizing an invader, the underlying biophysical mechanism has not been determined.

The list of top-25 proteins identified with MicroFlow was used to generate a histogram of MicroFlow and NanoFlow results ordered by total spectral counts (Figure 5). The histogram shows the average and standard deviation of 3 repeats on a single sample. The four proteins that differed between MicroFlow and NanoFlow were both identified by the other method, but were not within the top-25 most abundant proteins. For example, carboxypeptidase B2 and alpha-2-HS-glycoprotein were the 23th and 25th most abundant proteins identified by MicroFlow and the 27th and 28th most abundant identified by NanoFlow. The proteomics data have been deposited to the ProteomeXchange Consortium via the PRIDE partner repository with the dataset identifier PXD01911 [64].

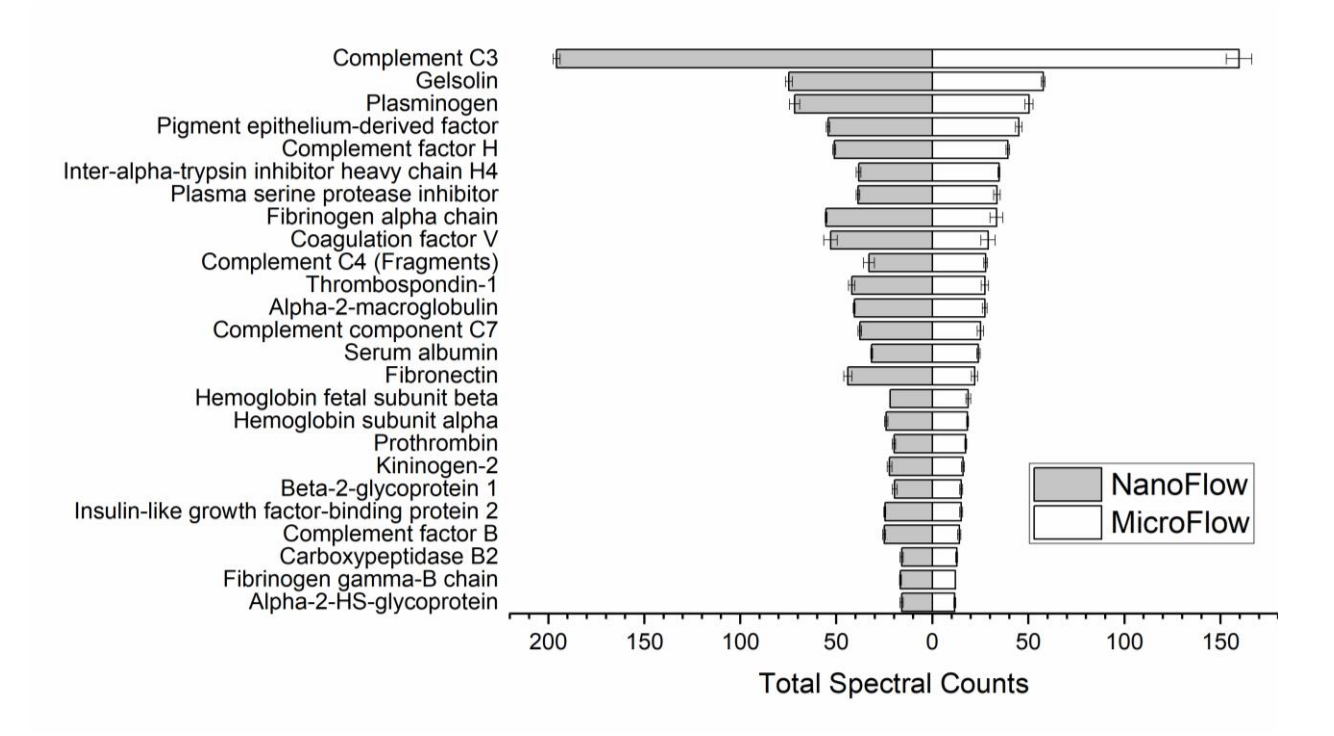


Figure 5. Comparison of total spectral counts obtained with low-cost MicroFlow LC (white) and standard NanoFlow LC (gray). The same biological sample was used for each LC method. The mean and standard deviation are shown for n=3 technical replicates. The complete data sets have been uploaded to the ProteomeXchange with the identifier PXD019118.

The downside of the faster flow system is the need for larger amounts of sample and identification of fewer proteins. Our proteomics core facility, and likely others, requests 5 µg of protein/sample for NanoFlow compared to 20 µg of protein/sample for MicroFlow. The slower flow rate of NanoFlow LC does mean that more proteins will be identified. For the polystyrene NPs, MicroFlow LC identified an average of 87 proteins, compared to 137 with standard NanoFlow LC. The 50 proteins that were not detected with MicroFlow LC had relatively low spectral counts. For example, NanoFlow LC results in 196 total spectral counts for complement C3, the most abundant protein identified in the polystyrene NP hard corona, and 32 spectral counts for serum albumin. Ezrin, with 7.3 spectral counts, was the most abundant protein identified by NanoFlow that was not observed with MicroFlow. In our previous work with albumin and plasminogen, we observed that the most abundant proteins dominate the cellular interaction [41,44,52].

In conclusion, the ability to predict what proteins will be present in the corona of a given NP would save considerable time and money. The first step towards this goal is obtaining significantly larger data sets, which will require automation. We report the use of a liquid handling robot to form and isolate the protein corona (Figure 2 and 3). Protein NPs with embedded magnetic cores demonstrate that this automated workflow can be extended to other NPs (Figure 4 and Table 2). With the large data sets, there is still the challenge of the cost associated with proteomic analysis. To address that, we compared two LC separation methods. The faster speed of MicroFlow LC translates to lower cost, while still successfully identifying abundant corona proteins (Figure 5). We hope this work will aid other researchers in the acquisition of large protein corona data sets.

Acknowledgment

The authors thank Dhanya T. Jayaram and Gustavo Sosa Macias for assistance with experiments and NSF (CBET-1901579) and NIH (NIAID 2R01AI101047-06A1) for funding. The protein NP TEM work was performed at the Georgia Tech Institute for Electronics and Nanotechnology, a member of the National Nanotechnology Coordinated Infrastructure, which is supported by the National Science Foundation (ECCS-1542174). We thank the Duke University School of Medicine for the use of the Proteomics and Metabolomics Shared Resource, which provided proteomics service, with special thanks to Erik Soderblom for discussion and technical advice.

Conflict of Interest

The authors have no conflicts of interest to report.

References

- 1. Lynch I, Cedervall T, Lundqvist M, Cabaleiro-Lago C, Linse S, Dawson KA. The nanoparticle protein complex as a biological entity; a complex fluids and surface science challenge for the 21st century. Adv Colloid Interfac. 2007; 134-135:167-174.
- 2. Walczyk D, Bombelli FB, Monopoli MP, Lynch I, Dawson KA. What the cell "sees" in bionanoscience. J Am Chem Soc. 2010; 132:5761-5768.
- 3. Park S, Hamad-Schifferli K. Nanoscale interfaces to biology. Curr Opin Chem Biol. 2010; 14:616-622.
- 4. Walkey CD, Chan WCW. Understanding and controlling the interaction of nanomaterials with proteins in a physiological environment. Chem Soc Rev. 2012; 41:2780-2799.
- 5. Del Pino P, Pelaz B, Zhang Q, Maffre P, Nienhaus GU, Parak WJ. Protein corona formation around nanoparticles from the past to the future. Mater Horiz. 2014; 1:301-313
- 6. Fleischer CC, Payne CK. Nanoparticle-cell interactions: Molecular structure of the protein corona and cellular outcomes. Acc Chem Res. 2014; 47:2651-2659.
- 7. Ke PC, Lin S, Parak WJ, Davis TP, Caruso F. A decade of the protein corona. ACS Nano. 2017; 11:11773-11776.
- 8. Mahmoudi M, Bertrand N, Zope H, Farokhzad OC. Emerging understanding of the protein corona at the nano-bio interfaces. Nano Today. 2016; 11:817-832.
- 9. Yang ST, Liu Y, Wang YW, Cao AN. Biosafety and Bioapplication of Nanomaterials by Designing Protein-Nanoparticle Interactions. Small. 2013; 9:1635-1653.
- 10. Payne CK. A protein corona primer for physical chemists. J Chem Phys. 2019; 151:130901.
- 11. Aggarwal P, Hall JB, McLeland CB, Dobrovolskaia MA, McNeil SE. Nanoparticle interaction with plasma proteins as it relates to particle biodistribution, biocompatibility and therapeutic efficacy. Adv Drug Deliver Rev. 2009; 61:428-437.
- 12. Owens III DE, Peppas NA. Opsonization, biodistribution, and pharmacokinetics of polymeric nanoparticles. Int J Pharm. 2006; 307:93-102.
- 13. Khlebtsov N, Dykman L. Biodistribution and toxicity of engineered gold nanoparticles: a review of in vitro and in vivo studies. Chem Soc Rev. 2011; 40:1647-1671.
- 14. Duan XP, Li YP. Physicochemical Characteristics of Nanoparticles Affect Circulation, Biodistribution, Cellular Internalization, and Trafficking. Small. 2013; 9:1521-1532.
- 15. Chinen AB, Guan CM, Ko CH, Mirkin CA. The Impact of Protein Corona Formation on the Macrophage Cellular Uptake and Biodistribution of Spherical Nucleic Acids. Small. 2017; 13:#1603847.
- 16. Wilhelm S, Tavares AJ, Dai Q, Ohta S, Audet J, Dvorak HF, Chan WC. Analysis of nanoparticle delivery to tumours. Nat Rev Mater. 2016; 1:16014.
- 17. Hellstrand E, Lynch I, Andersson A, Drakenberg T, Dahlbäck B, Dawson KA, Linse S, Cedervall T. Complete high-density lipoproteins in nanoparticle corona. FEBS J. 2009; 276:3372-3381.
- 18. Olenick LL, Troiano JM, Vartanian A, Melby ES, Mensch AC, Zhang L, Hong J, Mesele O, Qiu T, Bozich J. Lipid Corona Formation from Nanoparticle Interactions with Bilayers. Chem. 2018; 4:2709-2723.

- 19. Pink M, Verma N, Kersch C, Schmitz-Spanke S. Identification and characterization of small organic compounds within the corona formed around engineered nanoparticles. Environ Sci Nano. 2018; 5:1420-1427.
- 20. Khot LR, Sankaran S, Maja JM, Ehsani R, Schuster EW. Applications of nanomaterials in agricultural production and crop protection: A review. Crop Protection. 2012; 35:64-70.
- 21. Liu R, Lal R. Potentials of engineered nanoparticles as fertilizers for increasing agronomic productions. Sci Total Environ. 2015; 514:131-139.
- 22. Kah M, Hofmann T. Nanopesticide research: Current trends and future priorities. Environ Int. 2014; 63:224-235.
- 23. Giraldo JP, Wu HH, Newkirk GM, Kruss S. Nanobiotechnology approaches for engineering smart plant sensors. Nat Nanotechnol. 2019; 14:541-553.
- 24. Hochella MF, Mogk DW, Ranville J, Allen IC, Luther GW, Marr LC, McGrail BP, Murayama M, Qafoku NP, Rosso KM, Sahai N, Schroeder PA, Vikesland P, Westerhoff P, Yang Y. Natural, incidental, and engineered nanomaterials and their impacts on the Earth system. Science. 2019; 363:eaau8299.
- 25. Mauter MS, Zucker I, Perreault F, Werber JR, Kim JH, Elimelech M. The role of nanotechnology in tackling global water challenges. Nat Sustain. 2018; 1:166-175.
- 26. Kaegi R, Voegelin A, Sinnet B, Zuleeg S, Siegrist H, Burkhardt M. Transformation of AgCl nanoparticles in a sewer system A field study. Sci Total Environ. 2015; 535:20-27.
- 27. Lopez H, Lobaskin V. Coarse-grained model of adsorption of blood plasma proteins onto nanoparticles. J Chem Phys. 2015; 143:#243138.
- 28. Voicescu M, Ionescu S, Angelescu DG. Spectroscopic and coarse-grained simulation studies of the BSA and HSA protein adsorption on silver nanoparticles. J Nanopart Res. 2012; 14:1174.
- 29. Ding F, Radic S, Chen R, Chen P, Geitner NK, Brown JM, Ke PC. Direct observation of a single nanoparticle—ubiquitin corona formation. Nanoscale. 2013; 5:9162-9169.
- 30. Wei S, Ahlstrom LS, Brooks CL. Exploring protein–nanoparticle interactions with coarse-grained protein folding models. Small. 2017; 13:#1603748.
- 31. Ding H-M, Ma Y-Q. Computer simulation of the role of protein corona in cellular delivery of nanoparticles. Biomaterials. 2014; 35:8703-8710.
- 32. Li R, Chen R, Chen P, Wen Y, Ke PC, Cho SS. Computational and experimental characterizations of silver nanoparticle–apolipoprotein biocorona. J Phys Chem B. 2013; 117:13451-13456.
- 33. Li R, Stevens CA, Cho SS (2017) Molecular Dynamics Simulations of Biocorona Formation. In: Suzuki J, Nakano T, Moore MJ (eds) Modeling, Methodologies and Tools for Molecular and Nano-scale Communications: Modeling, Methodologies and Tools. Springer International Publishing, p. 241-256.
- 34. Manning MD, Kwansa AL, Oweida T, Peerless JS, Singh A, Yingling YG. Progress in ligand design for monolayer-protected nanoparticles for nanobio interfaces. Biointerphases. 2018; 13:06D502.
- 35. Deyev S, Proshkina G, Ryabova A, Tavanti F, Menziani MC, Eidelshtein G, Avishai G, Kotlyar A. Synthesis, Characterization, and Selective Delivery of DARPin–Gold Nanoparticle Conjugates to Cancer Cells. Bioconj Chem. 2017; 28:2569-2574.

- 36. Tavanti F, Pedone A, Menziani MC. Competitive binding of proteins to gold nanoparticles disclosed by molecular dynamics simulations. J Phys Chem C. 2015; 119:22172-22180.
- 37. Cui Q, Hernandez R, Mason SE, Frauenheim T, Pedersen JA, Geiger F. Sustainable nanotechnology: opportunities and challenges for theoretical/computational studies. J Phys Chem B. 2016; 120:7297-7306.
- 38. Liang D, Hong J, Fang D, Bennett JW, Mason SE, Hamers RJ, Cui Q. Analysis of the conformational properties of amine ligands at the gold/water interface with QM, MM and QM/MM simulations. Phys Chem Chem Phys. 2018; 20:3349-3362.
- 39. Van Lehn RC, Alexander-Katz A. Structure of mixed-monolayer-protected nanoparticles in aqueous salt solution from atomistic molecular dynamics simulations. J Phys Chem C. 2013; 117:20104-20115.
- 40. Brancolini G, Maschio MC, Cantarutti C, Corazza A, Fogolari F, Bellotti V, Corni S, Esposito G. Citrate stabilized gold nanoparticles interfere with amyloid fibril formation: D76N and Δ N6 β 2-microglobulin variants. Nanoscale. 2018; 10:4793-4806.
- 41. Fleischer CC, Payne CK. Nanoparticle surface charge mediates the cellular receptors used by protein-nanoparticle complexes. J Phys Chem B. 2012; 116:8901-8907.
- 42. Fleischer CC, Kumar U, Payne CK. Cellular binding of anionic nanoparticles is inhibited by serum proteins independent of nanoparticle composition. Biomat Sci. 2013; 1:975-982.
- 43. Fleischer CC, Payne CK. Secondary structure of corona proteins determines the cell surface receptors used by nanoparticles. J Phys Chem B. 2014; 118:14017-14026.
- 44. Hill A, Payne CK. Impact of serum proteins on MRI contrast agents: Cellular binding and T2 relaxation. RSC Adv. 2014; 4:31735-31744.
- 45. Walkey CD, Olsen JB, Song F, Liu R, Guo H, Olsen DWH, Cohen Y, Emili A, Chan WC. Protein corona fingerprinting predicts the cellular interaction of gold and silver nanoparticles. ACS Nano. 2014; 8:2439-2455.
- 46. Findlay MR, Freitas DN, Mobed-Miremadi M, Wheeler KE. Machine learning provides predictive analysis into silver nanoparticle protein corona formation from physicochemical properties. Environ Sci Nano. 2018; 5:64-71.
- 47. Lazarovits J, Sindhwani S, Tavares AJ, Zhang Y, Song F, Audet J, Krieger JR, Syed AM, Stordy B, Chan WC. Supervised learning and mass spectrometry predicts the in vivo fate of nanomaterials. ACS Nano. 2019; 13:8023-8034.
- 48. Chan EM, Xu C, Mao AW, Han G, Owen JS, Cohen BE, Milliron DJ. Reproducible, high-throughput synthesis of colloidal nanocrystals for optimization in multidimensional parameter space. Nano Lett. 2010; 10:1874-1885.
- 49. Pendleton IM, Cattabriga G, Li Z, Najeeb MA, Friedler SA, Norquist AJ, Chan EM, Schrier J. Experiment Specification, Capture and Laboratory Automation Technology (ESCALATE): a software pipeline for automated chemical experimentation and data management. MRS Communications. 2019; 9:846-859.
- 50. Runa S, Khanal D, Kemp ML, Payne CK. TiO2 nanoparticles alter the expression of peroxiredoxin antioxidant genes. J Phys Chem C. 2016; 120:20736-20742.
- 51. Jayaram DT, Runa S, Kemp ML, Payne CK. Nanoparticle-induced oxidation of corona proteins initiates an oxidative stress response in cells. Nanoscale. 2017; 9:7595-7601.
- 52. Jayaram DT, Pustulka SM, Mannino RG, Lam WA. Protein corona in response to flow: Effect on protein concentration and structure. Biophysical J. 2018; 115:209-216.

- 53. Jayaram DT, Kumar A, Kippner LE, Ho P-Y, Kemp ML, Fan Y, Payne CK. TiO 2 nanoparticles generate superoxide and alter gene expression in human lung cells. RSC Adv. 2019; 9:25039-25047.
- 54. Etorki AM, Gao M, Sadeghi R, Maldonado-mejia LF, Kokini JL. Effects of Desolvating Agent Types , Ratios , and Temperature on Size and Nanostructure of Nanoparticles from α-Lactalbumin and Ovalbumin. J Food Sci. 2016; 81:E2511-E2520.
- 55. Chang TZ, Stadmiller SS, Staskevicius E, Champion JA. Effects of ovalbumin protein nanoparticle vaccine size and coating on dendritic cell processing. Biomat Sci. 2017; 5:223-233.
- 56. Schneider CA, Rasband WS, Eliceiri KW. NIH Image to ImageJ: 25 years of image analysis. Nat Methods. 2012; 9:671.
- 57. Rimkus G, Bremer-Streck S, Grüttner C, Kaiser WA, Hilger I. Can we accurately quantify nanoparticle associated proteins when constructing high-affinity MRI molecular imaging probes? Contrast Media Molec. Imaging. 2011; 6:119-125.
- 58. Gruttner C, Muller K, Teller J. A rapid assay to measure the shielding of iron oxide cores by the particle shell. IEEE Trans Magn. 2012; 49:177-181.
- 59. Muller J, Bauer KN, Prozeller D, Simon J, Mailander V, Wurm FM, Winzen S, Landfester K. Coating nanoparticles with tunable surfactants facilitates control over the protein corona. Biomaterials. 2017; 115:1-8.
- 60. Chang TZ, Diambou I, Rok J, Baozhong K, Champion JA. Host- and Pathogen-Derived Adjuvant Coatings on Protein Nanoparticle Vaccines. Bioeng Transl Med. 2017; 2:120-130.
- 61. Deng L, Mohan T, Chang TZ, Gonzalez GX, Wang Y, Kwon Y, Kang S, Compans RW, Champion JA, Wang B. Double-layerd protein nanoparticles induce broad protection against divergent influenza A viruses. Nature Commun. 2018; 9:1-12.
- 62. Sakulkhu U, Maurizi L, Mahmoudi M, Motazacker M, Vries M, Gramoun A, Beuzelin M-GO, Vallée J-P, Rezaee F, Hofmann H. Ex situ evaluation of the composition of protein corona of intravenously injected superparamagnetic nanoparticles in rats. Nanoscale. 2014; 6:11439-11450.
- 63. Chen F, Wang G, Griffin JI, Brenneman B, Banda NK, Holers VM, Backos DS, Wu L, Moghimi SM, Simberg D. Complement proteins bind to nanoparticle protein corona and undergo dynamic exchange in vivo. Nat Nanotechnol. 2017; 12:387.
- 64. Vizcaíno JA, Deutsch EW, Wang R, Csordas A, Reisinger F, Rios D, Dianes JA, Sun Z, Farrah T, Bandeira N. ProteomeXchange provides globally coordinated proteomics data submission and dissemination. Nat Biotechnol. 2014; 32:223-226.